Structure-Based Design of a Fusion Glycoprotein Vaccine for Respiratory Syncytial Virus

Jason S. McLellan *et al.*

Science **342**, 592 (2013);
DOI: 10.1126/science.1243283

Science (print ISSN 0036-8075; online ISSN 1095-9203) is published weekly, except the last week in December, by the American Association for the Advancement of Science, 1200 New York Avenue NW, Washington, DC 20005.

Structure-Based Design of a Fusion Glycoprotein Vaccine for Respiratory Syncytial Virus

Jason S. McLellan,[1] Man Chen,[1]* M. Gordon Joyce,[1]* Mallika Sastry,[1]* Guillaume B. E. Stewart-Jones,[1]* Yongping Yang,[1]* Baoshan Zhang,[1]* Lei Chen,[1] Sanjay Srivatsan,[1] Anqi Zheng,[1] Tongqing Zhou,[1] Kevin W. Graepel,[1] Azad Kumar,[1] Syed Moin,[1] Jeffrey C. Boyington,[1] Gwo-Yu Chuang,[1] Cinque Soto,[1] Ulrich Baxa,[2] Arjen Q. Bakker,[3] Hergen Spits,[3] Tim Beaumont,[3] Zizheng Zheng,[4] Ningshao Xia,[4] Sung-Youl Ko,[1] John-Paul Todd,[1] Srinivas Rao,[1] Barney S. Graham,[1]† Peter D. Kwong[1]†

Respiratory syncytial virus (RSV) is the leading cause of hospitalization for children under 5 years of age. We sought to engineer a viral antigen that provides greater protection than currently available vaccines and focused on antigenic site Ø, a metastable site specific to the prefusion state of the RSV fusion (F) glycoprotein, as this site is targeted by extremely potent RSV-neutralizing antibodies. Structure-based design yielded stabilized versions of RSV F that maintained antigenic site Ø when exposed to extremes of pH, osmolality, and temperature. Six RSV F crystal structures provided atomic-level data on how introduced cysteine residues and filled hydrophobic cavities improved stability. Immunization with site Ø–stabilized variants of RSV F in mice and macaques elicited levels of RSV-specific neutralizing activity many times the protective threshold.

Respiratory syncytial virus (RSV) is one of the last remaining highly prevalent childhood pathogens without an approved vaccine. It is estimated to be responsible for 6.7% of deaths in children 1 month to 1 year of age and causes excess mortality in the elderly at levels comparable to influenza virus (*1*). Although RSV infection does not induce fully protective immunity, antibodies against the RSV fusion (F) glycoprotein can prevent severe disease in humans as demonstrated by passive prophylaxis with the F-directed antibody, palivizumab (Synagis) (*2*).

The proven success of palivizumab (*3*) has spurred vaccine efforts aimed at eliciting protective RSV F–directed antibodies. These efforts have been complicated by the conformational diversity of RSV F (*4*–*8*), a type I fusion glycoprotein that merges virus and host-cell membranes by using the difference in folding energy between two substantially different states: a metastable state adopted before virus-cell interaction (prefusion) and a stable state that occurs after merging of virus and cell membranes (postfusion). Both states exhibit epitopes targeted by neutralizing antibodies, and postfusion RSV F is being developed as a vaccine candidate (*6*, *9*). Recently, however, the major target of RSV-neutralizing antibodies elicited by natural infection was found to reside primarily on the prefusion conformation of RSV F (*10*). Antibodies such as 5C4 (*7*), AM22, and D25 (*11*, *12*) are substantially more potent than palivizumab and target antigenic site Ø (zero), a metastable site located at the membrane-distal apex of the prefusion RSV F trimer (*7*).

To enhance elicitation of similarly potent antibodies, we engineered soluble variants of RSV F with stably exposed antigenic site Ø. These variants were characterized antigenically and crystallographically and tested for immunogenicity in mice and nonhuman primates (rhesus macaques).

Structure-Based Vaccine Strategy

We and others have engineered antigenicity (*13*–*17*) through structure-based design of the epitopes recognized by template neutralizing antibodies. For example, the crystal structure of motavizumab (a variant of palivizumab) bound to its F glycoprotein epitope (*18*) allowed us to create epitope scaffolds, which stably presented the motavizumab epitope on heterologous proteins (*19*). Although motavizumab-epitope scaffolds could elicit immune responses that recognized F, substantial neutralizing activity was not induced (*19*). We hypothesized that instead of a single epitope recognized by a single template antibody, it would be advantageous to present a "supersite" (*20*), comprising a collection of overlapping epitopes recognized by multiple antibodies. Even more preferable would be for such a site to be ultrasensitive to neutralization. These considerations led to a "neutralization-sensitive site" strategy: (i) to identify a viral site targeted by multiple antibodies with extremely potent neutralizing activity, (ii) to determine the structure of the site in complex with a representative antibody, (iii) to engineer the stable presentation of the site in the absence of recognizing antibody, and (iv) to elicit high-titer protective responses through immunization with engineered antigens that stably present the neutralization-sensitive site (fig. S1).

Engineering of RSV F Antigens

Antigenic site Ø was chosen as the target site because of its recognition by RSV-neutralizing antibodies that are 10- to 100-fold more potent than palivizumab (*7*, *11*, *12*). We previously determined the structure of antigenic site Ø in complex with the D25 antibody (*7*). Structure determination involved appending the T4-phage fibritin trimerization domain ("foldon") (*21*, *22*) to the C terminus of the RSV F ectodomain (*5*) and binding of the prefusion-specific D25 antibody. Although these approaches stabilized antigenic site Ø, D25 binding sterically occluded the target site. To stably present antigenic site Ø in the absence of D25, we retained the C-terminal trimerization domain and combined it with other means of stabilization, including the introduction of cysteine pairs or cavity-filling hydrophobic substitutions.

The β-carbons of serine residues 155 and 290 are 4.4 Å apart in the D25-bound RSV F structure (*7*) and 124.2 Å apart in the postfusion structure (*5*) (Fig. 1 and fig. S2). A S155C-S290C double mutant (DS) [in which cysteine replaced serine at positions 155 and 290 (*23*)] formed stable RSV F trimers, expressed at 1.4 mg/liter, retained antigenic site Ø, and was homogeneous as judged by negative-stain electron microscopy (Table 1 and fig. S3) (*24*, *25*). Other intrachain cysteine modifications, such as those between regions of RSV F that do not rearrange between pre- and postfusion states (e.g., S403C and T420C), did not stabilize antigenic site Ø (Table 1). We also tested potential interchain double-cysteine modifications, but none expressed at levels sufficient for enzyme-linked immunosorbent assay (ELISA) detection (table S1) (*26*).

We analyzed the D25-bound RSV F structure for hydrophobic cavities unique to the D25-bound conformation of RSV F that abutted regions that differed in the prefusion and postfusion states (*27*). Several such cavities were identified in the membrane-distal "head" of the prefusion structure, close to the binding site of D25, and we engineered hydrophobic substitutions to fill these cavities. S190F and V207L substitutions were predicted to adopt prevalent side-chain conformations with minimal clashes, whereas K87F, V90L, V220L, and V296F showed less steric compatibility. We assessed the impact of filling these cavities with pairs of changed residues. A S190F-V207L pair (Cav1) (Fig. 1), formed stable RSV F trimers, expressed at 2.2 mg/liter, and retained antigenic site Ø (Table 1). Moreover, K87F-V90L, S190F-

[1]Vaccine Research Center, National Institute of Allergy and Infectious Diseases, National Institutes of Health, Bethesda, MD 20892, USA. [2]Electron Microscopy Laboratory, Advanced Technology Program, SAIC-Frederick, Inc., Frederick National Laboratory for Cancer Research, Frederick, MD 21702, USA. [3]AIMM Therapeutics, Academic Medical Center, 1105 BA Amsterdam, Netherlands. [4]National Institute of Diagnostics and Vaccine Development in Infectious Diseases, Xiamen University, Xiamen, 361005, China.

*These authors contributed equally to this work.
†Corresponding author. E-mail: bgraham@nih.gov (B.S.G.); pdkwong@nih.gov (P.D.K.)

V296F, and V207L-V220L variants showed enhanced retention of D25 recognition but expressed at less than 0.1 mg/liter (Table 1).

Other cavities we identified toward the center of prefusion RSV F were close to the fusion peptide, the trimer axis, and an acidic patch comprising residues Asp^{486}, Glu^{487}, and Asp^{489}. We modeled several cavity-filling substitutions, including F137W, F140W, and F488W, and analyzed these substitutions in combination with D486H, E487Q, and D489H (table S1). Of the six combinations tested, only two (F488W and D486H-E487Q-F488W-D489H) expressed levels of purified RSV F trimer at greater than 0.1 mg/liter and retained D25 recognition. The D486H-E487Q-F488W-D489H variant (TriC) formed stable RSV F trimers, expressed at 0.8 mg/liter, and retained antigenic site Ø (Fig. 1 and Table 1).

We also tested the impact of destabilizing the postfusion conformation on the preservation of antigenic site Ø. The substitution V178N, which is predicted to introduce an *N*-linked glycan compatible with the prefusion but not the postfusion conformation of F, did not appear to stabilize antigenic site Ø, nor did V185E or I506K, which were predicted to place a glutamic acid or a lysine into the interior of the postfusion six-helix bundle (Table 1). In all, more than 100 RSV F variants were constructed (table S1), expressed in a 96-well transfection format (*28*) (fig. S4), and tested by ELISA of the culture supernatants for binding to D25 and motavizumab (figs. S5 and S6). Fifteen constructs were compatible with D25 binding, four of which retained D25 recognition for at least 7 days at 4°C, and three of these could be purified as homogeneous trimers that retained antigenic site Ø (table S1 and fig. S7). Overall, we observed a strong correlation between retention of D25 binding for at least 7 days at 4°C in 96-well supernatants and yield of purified trimers after large-scale expression and purification (fig. S5).

Combinatorial Optimization of Site Ø Stability

DS, Cav1, and TriC variants displayed a variety of physical and antigenic properties. The DS variant was the least stable to pH and temperature variation but was more permanently stabilized in the trimeric state, whereas a low level of continual conversion from trimer to aggregate was observed for Cav1 and TriC on size-exclusion chromatography. Combinations of the three variants improved retention of D25 reactivity to physical extremes, a characteristic helpful to manufacturing. Overall, the DS-Cav1 combination appeared optimal in terms of trimer yield and physical stability to extremes of temperature, pH, osmolality, and freeze-thaw (Table 1), and was homogeneous as judged by negative-stain electron microscopy (fig. S2).

Crystallographic Analysis

To provide atomic-level information, we determined crystal structures of site Ø–stabilized variants of RSV F (Fig. 2). The DS, Cav1, DS-Cav1, and DS-Cav1-TriC variants all crystallized in similar 1.5 M tartrate (pH 9.5) conditions, and these cubic crystals diffracted x-rays to resolutions of 3.2 Å, 3.1 Å, 3.1 Å, and 2.8 Å, respectively (table S2). Molecular replacement solutions were obtained by using the D25-bound RSV F structure as a search model, and these revealed a single RSV F protomer in the asymmetric unit, with the trimeric F axis aligned along the crystallographic three-fold axis. Tetragonal crystals of Cav1 and cubic crystals of DS-Cav1 were also obtained from 1.7 M ammonium sulfate (pH 5.5) conditions, and these diffracted to resolutions of 2.4 Å and 3.0 Å, respectively (table S2). Molecular replacement revealed the tetragonal lattice to have a full RSV F trimer in the asymmetric unit and to be highly related to the tartrate cubic lattices. Overall, these structures revealed the engineered RSV F variants to be substantially in the D25-bound conformation (*29*).

Although the structure of the DS variant (Fig. 2, left column) revealed that the cysteine-substituted residues at 155 and 290 formed a disulfide bond that prevented triggering to the postfusion state, much of the membrane-distal portion of the RSV F trimer, including antigenic site Ø, was either disordered (residues 63 to 72 and 169 to 216) or in a different conformation. Thus, for example, residues 160 to 168 in the DS structure extended the α2 helix instead of forming a turn and initiating the α3 helix, as in the D25-bound F structure (Fig. 2C, left). One possible explanation for the differences between the DS structure and the D25-bound RSV F structure is that antigenic site Ø in DS is flexible and crystallized in a conformation that does not bind D25 (*30*). Overall, the DS variant retained many of the features of the prefusion state of RSV F, including the fusion peptide in the interior of the trimeric cavity; however, it failed to fix antigenic site Ø in its D25-bound conformation (fig. S8).

In comparison with DS, the Cav1 structure (Fig. 2, second and third columns) was more ordered at its membrane-distal apex, with α3 helix, β3/β4 hairpin, and α4 helix clearly defined. Residues 137 to 202, which contain the S190F substitution, had a Cα root mean square deviation of 0.6 Å when compared with the D25-bound F structure. The higher degree of structural order was likely due to the S190F mutation that filled a cavity observed in the D25-bound F structure and increased van der Waals contacts with residues Ile^{57}, Lys^{176}, Val^{192}, Glu^{256}, Ser^{259}, and Leu^{260}. The other cavity-filling mutation in Cav1, V207L, was shifted by 5.5 Å compared with the D25-bound F structure, with the C-terminal portion of the

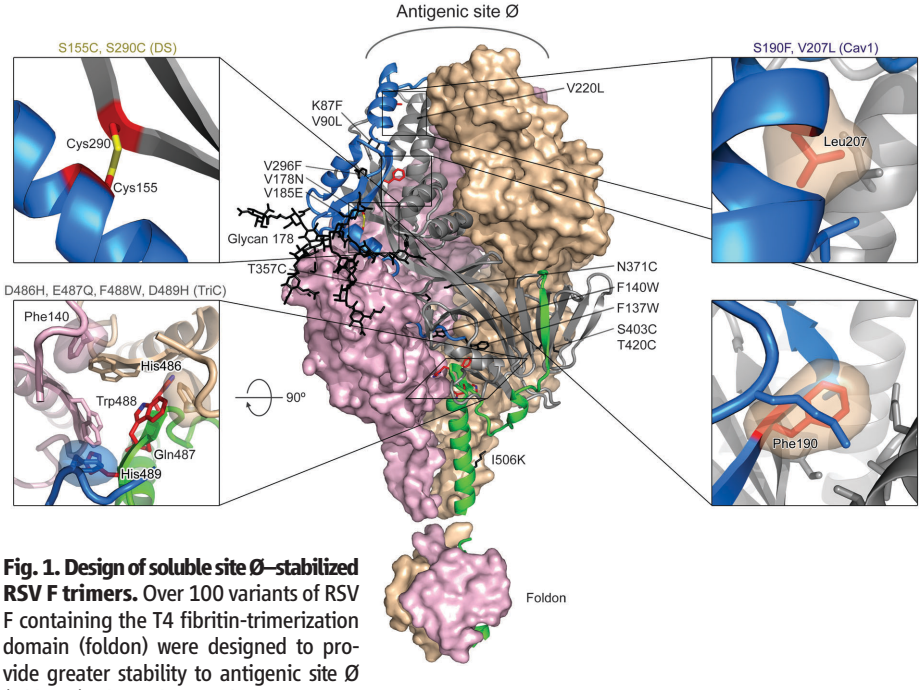

Fig. 1. Design of soluble site Ø–stabilized RSV F trimers. Over 100 variants of RSV F containing the T4 fibritin-trimerization domain (foldon) were designed to provide greater stability to antigenic site Ø (table S1). Shown here is the structure of the RSV F trimer in its D25-bound conformation with modeled C-terminal foldon. The trimer is displayed with two of the three F_1F_2 protomers in molecular surface representation (colored tan and pink), and the third F_1F_2 protomer in ribbon representation. The ribbon is colored gray in regions where it is relatively fixed between pre- and postfusion, and the N- and C-terminal residues that move more than 5 Å between pre- and postfusion conformations are colored blue and green, respectively. Mutations compatible with RSV F expression and initial D25 recognition (table S1), but insufficiently stable to allow purification of RSV F as a homogenous trimer (Table 1), are labeled and shown in stick representation (colored black). Insets show enlargements of stabilizing mutations in stick representation (colored red) for DS, Cav1, and TriC variants, all of which sufficiently stabilize antigenic site Ø to allow purification as a homogeneous trimer (Table 1).

α4 helix kinking near Pro^{205} and adopting distinct conformations in the two crystallization conditions (Fig. 2, second and third columns), which suggested that the V207L mutation is unable to stabilize the α4 helix in the D25-bound conformation.

A striking feature of the Cav1 structure in the tetragonal crystal lattice was the C terminus of F_2, which is disordered in the D25-bound F structure, but in Cav1, tunnels into the trimeric cavity alongside the fusion peptide. We also observed the C terminus to end with Ala^{107}, and not Arg^{109}, as expected after cleavage of the furin site (Arg^{106}-Ala^{107}-Arg^{108}-Arg^{109}) (*31*). In the Cav1 structure, the positive charge of Arg^{106} was offset by an ordered sulfate ion (Fig. 2C). Biologically, the interior position of the F_2 C terminus may play a role in triggering structural rearrangements of F.

Comparison of the DS-Cav1 structures from the two cubic crystal forms (Fig. 2, second and third columns from right) to those of Cav1 revealed only minor differences (*32*). The largest differences occurred at the RSV F apex, including antigenic site Ø and specifically at residues 64 to 73 and 203 to 216. Notably, the atomic mobility (*B*-factor) was highest in this apex region for all of the site Ø–stabilized variants, perhaps indicative of intrinsic site Ø flexibility. However, site Ø has low atomic mobility when bound by D25, which reveals the ability of D25 to stabilize both overall and local RSV F conformations.

The structure of the DS-Cav1-TriC triple combination (Fig. 2, far right column) was also highly similar to other Cav1-containing RSV F variant structures. One difference in the electron density corresponded to an expanse of weak density at the membrane-proximal region, which approximated the dimensions of the T4-fibritin trimerization domain (*33*) but was not visible in other crystallized RSV F structures containing this domain, including the D25-bound structure (*7*). Small structural differences in packing likely allowed for the partial ordering of this domain (and may also have accounted for the increased diffraction limit of the DS-Cav1-TriC crystals relative to the other cubic variants), rather than differences in the interaction between the DS-Cav1-TriC stabilized RSV F and the trimerization domain.

The critical F488W substitution in the TriC alteration of residues 486 to 489 packed directly against the F488W substitutions in neighboring protomers of the RSV F trimer. The indole side chain of Trp^{488} pointed toward the trimer apex and also formed ring-stacking interactions with the side chain of Phe^{140} of the fusion peptide (Fig. 2C, far right). This fusion peptide interaction, which is not observed in any of the Phe^{488}-containing structures, likely inhibits the extraction of the fusion peptide from the prefusion trimer cavity and thus provides a structural rationale for the ability of the F488W substitution to stabilize the prefusion state of RSV F (Table 1).

Immunogenicity of Antigenic Site Ø–Stabilized RSV F

To assess the effect of site Ø stabilization on the elicitation of RSV-protective humoral responses, we immunized CB6F1/J mice with various forms of RSV F, injecting each mouse with 10 μg RSV F combined with 50 μg polyinosinic-polycytidylic acid stabilized with polylysine carboxymethylcellulose (poly-ICLC) adjuvant at weeks 0 and 3, and measured the ability of week 5 sera to prevent RSV infection of HEp-2 cells. DS, Cav1, and TriC each elicited high titers of neutralizing activity [geometric mean 50% effective concentrations (EC_{50} values) of 1826 to 2422]. This level was ~4 times that elicited by postfusion F (504 EC_{50}), and ~20 times the protective threshold (*34*). By comparison, DS-Cav1 elicited neutralizing activity of 3937 EC_{50}, roughly 8 times that of postfusion F and 40 times the protective threshold (*34*) (Fig. 3A).

To quantify antibody responses to different sites on prefusion RSV F, we used antigenic site Ø–occluded forms of RSV F. CB6F1/J mice immunized with 20 μg RSV F bound by antigenic site Ø–directed antibodies (comprising ~10 μg of RSV F and ~10 μg of the antigen-binding fragment of antibody) developed at week 5 geometric

Table 1. Antigenic and physical properties of engineered RSV F glycoprotein variants. Variants were often observed to exist in a mixture of oligomeric states on size-exclusion chromatography. If a measureable trimeric fraction was observed, then this is indicated by the label "Trimer," and the various properties of the trimer fraction are listed. If no trimeric fraction was observed, then the oligomeric state of the dominant oligomeric species is provided. If the total yield before size-exclusion chromatography was <0.1 mg/liter, then oligomeric state is listed as not determined (N.D.). Yield shown is for the specified oligomeric state. When no binding was observed for 1 μM Fab, the K_D is shown as >1000 nM; when total yield was <0.1 mg/liter, then the value for K_D is not applicable (N/A). For site II, palivizumab (Paliv); motavizumab (Mota). Physical stability refers to D25 reactivity retained after exposure to various physical extremes. There were 10 cycles of freeze-thaw. N/A, not applicable.

Mechanism of stabilization	RSV F variant	Oligomeric state	Yield (mg/liter)	Antibody K_D value (nM)							Physical stability (fractional D25 reactivity)						
				Site Ø			Site I	Site II		Site IV	Temp (°C)		pH		Osmolality (mM)		Freeze-thaw
				D25	AM22	5C4	131-2a	Paliv	Mota	101F	50	70	3.5	10.0	10	3000	
Cavity filling	K87F-V90L	Aggregate	0.3	>1000	>1000	>1000	7.6	1.7	0.17	1.6	N/A	N/A	N/A	N/A	N/A	N/A	N/A
	F137W-F140W	N.D.	<0.1	N/A	N/A	N/A	N/A	N/A	N/A	N/A	N/A	N/A	N/A	N/A	N/A	N/A	N/A
	F137W-F140W-F488W	N.D.	<0.1	N/A	N/A	N/A	N/A	N/A	N/A	N/A	N/A	N/A	N/A	N/A	N/A	N/A	N/A
	S190F-V207L (Cav1)	Trimer	2.2	0.23	<0.10	9.3	>1000	43	<0.01	2.9	0.8	0.1	0.7	0.8	1.0	0.7	0.6
	S190F-V296F	Aggregate	0.4	>1000	>1000	>1000	4.2	1.7	<0.01	1.6	N/A	N/A	N/A	N/A	N/A	N/A	N/A
	V207L-V220L	Aggregate	0.4	>1000	>1000	>1000	2.8	0.99	0.014	0.69	N/A	N/A	N/A	N/A	N/A	N/A	N/A
	D486H-E487Q-F488W-D489H (TriC)	Trimer	0.8	0.012	1.0	34	>1000	31	0.48	4.0	0.8	0.1	0.1	0.8	1.3	0.6	0.1
	F488W	Trimer	1.7	0.087	0.25	27	>1000	32	0.1	4.7	0.9	0.1	0.1	0.7	1.1	0.5	0
Disulfide formation	S155C-S290C (DS)	Trimer	1.4	0.29	<0.01	35	3.4	2.8	0.043	2.2	0.3	0	0.1	0.8	1.3	0.8	0.3
	T357C-N371C	N.D.	<0.1	N/A	N/A	N/A	N/A	N/A	N/A	N/A	N/A	N/A	N/A	N/A	N/A	N/A	N/A
	S403C-T420C	Aggregate	0.3	>1000	>1000	>1000	3.05	3.3	0.05	1.85	N/A	N/A	N/A	N/A	N/A	N/A	N/A
N-Glycan addition	V178N	Aggregate	<0.1	>1000	>1000	>1000	7.2	3.1	0.11	1.64	N/A	N/A	N/A	N/A	N/A	N/A	N/A
Postfusion destabilization	V185E	Aggregate	<0.1	>1000	>1000	>1000	3.5	1.7	0.11	1.64	N/A	N/A	N/A	N/A	N/A	N/A	N/A
	I506K	Aggregate	<0.1	>1000	>1000	>1000	4.6	1.7	0.054	1.39	N/A	N/A	N/A	N/A	N/A	N/A	N/A
Acid patch neutralization	D486H-E487Q-D489H	Aggregate	0.1	>1000	>1000	>1000	>1000	9.5	0.57	12.7	N/A	N/A	N/A	N/A	N/A	N/A	N/A
Double combinations	DS-Cav1	Trimer	1.9	0.15	<0.01	13	>1000	23	0.041	3.2	0.9	0	0.8	0.9	1.0	0.8	0.7
	DS-TriC	Trimer	0.6	0.17	<0.01	33	2.0	4.8	0.055	3.1	0.9	0	0.3	0.9	0.5	0.9	0.5
	Cav1-TriC	Trimer	0.2	0.99	0.086	5.1	>1000	33	0.17	3.1	0.9	0.1	0.3	0.8	0.6	0.5	0
Triple combinations	DS-Cav1-TriC	Trimer	1.3	0.17	0.02	18	>1000	20	0.10	3.2	0.9	0.1	0.6	0.9	0.6	0.6	0

mean neutralizing titers of 911 and 1274 EC_{50} for AM22 and D25 complexes, respectively, roughly double that of postfusion at 10 μg/ml and comparable to those elicited by postfusion at 20 μg/ml (Fig. 3A). These findings suggested that the very high titers elicited by immunization with RSV F variants stabilized in the prefusion state, especially DS-Cav1, were a result of antibodies targeting antigenic site Ø.

To examine the generality of site Ø elicitation, we immunized rhesus macaques with DS-Cav1, DS, and postfusion forms of RSV F, injecting each macaque with 50 μg RSV F mixed with 500 μg poly-ICLC adjuvant at weeks 0 and 4 and measured the ability of week 2, 4, 6, 8, 10, and 14 sera to inhibit RSV infection. Formulated proteins retained their expected antigenic profiles as measured by D25 binding to material from the injectate (fig. S9). At week 6, DS and DS-Cav1 elicited geometric mean titers of 1222 and 2578 EC_{50}, respectively, roughly 5 and 10 times those of postfusion F (287 EC_{50}) (Fig. 3B). By week 8, geometric mean titers of DS-Cav1 were roughly 70 times those elicited by postfusion F against the homologous RSV subtype A and more than 80 times titers against RSV subtype B (fig. S10 and table S4). Overall, these results demonstrate a conservation of the relative immunogenicity for the different forms of RSV F immunogen between mice and primates, with DS-Cav1 eliciting RSV-protective titers many times the protective threshold in a primate immune system against both major RSV subtypes.

Optimization of RSV F Protective Responses

The interplay among design, physical and antigenic properties, atomic-level structure, and immunogenicity provides a basis for further optimization of RSV vaccine candidates (*35*). For example, to obtain insight into the relation between various antigenic and physical properties of engineered RSV Fs and the elicitation of RSV-protective

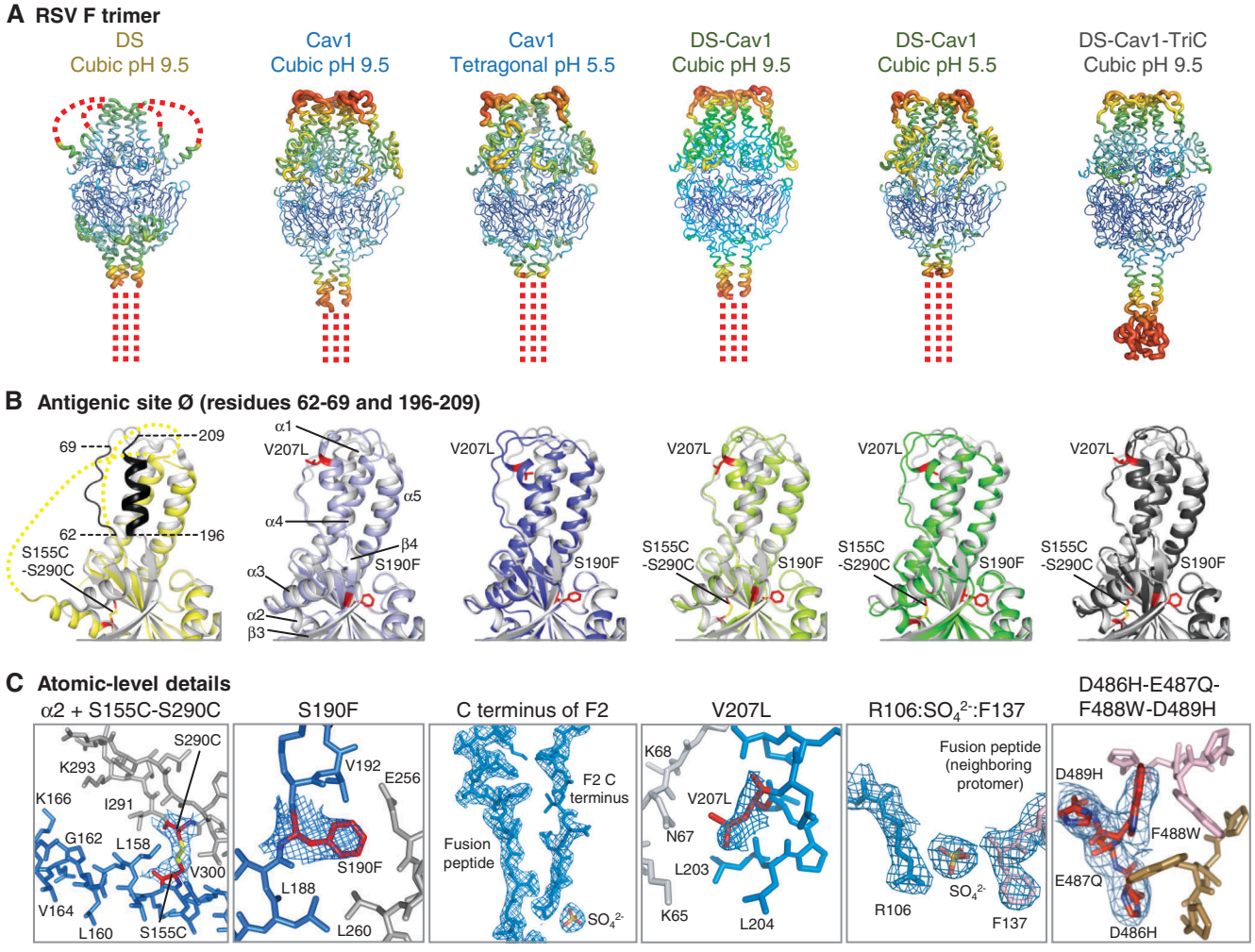

Fig. 2. Crystal structures of RSV F trimers, engineered to preserve antigenic site Ø. (A to **C)** Six structures for RSV F variants are shown, labeled by stabilizing mutation (DS, Cav1, DS-Cav1, and DS-Cav1-TriC) and the crystal lattice (cubic or tetragonal). (A) RSV F trimers are displayed in Cα-worm representation, colored according to atomic mobility factor, with regions of higher flexibility in warmer colors (red) and regions of lower flexibility in cooler colors (blue). Missing regions are shown as dotted lines. These occur at the C-terminal membrane-proximal region, where the foldon motif is not seen, except in the DS-Cav1-TriC structure (far right). In the DS structure, two loops in the head region are also disordered. (B) Antigenic site Ø of a RSV F protomer is displayed in ribbon diagram, with the structure of D25-bound RSV F in gray and different variants colored yellow (DS), light and dark blue (Cav1), light and dark green (DS-Cav1), and black (DS-Cav1-TriC). Residues corresponding to antigenic site Ø are highlighted in black on the image at far left, and secondary structural elements are shown on the second image from left. Stabilizing mutations are labeled and shown in stick representation (colored red). Perpendicular view presented in figure S8. (C) Atomic-level details are shown in stick representation, colored the same as in Fig. 2, with regions of RSV F that change conformation between prefusion and postfusion conformation in red and blue, and those that remain constant in gray. Carbon atoms for stabilizing mutations are colored red. In Cav1 (pH 5.5) and in DS-Cav1 (pH 5.5) novel features were observed involving the interaction of the C terminus of the F_2 peptide with a sulfate ion and the fusion peptide. In the DS-Cav1-TriC structure, the D486H-E487Q-F488W-D489H mutations interact with the two neighboring protomers (colored tan and pink) around the trimer axis.

responses, one can correlate antigenic and physical properties (Table 1) with immunogenicity (Fig. 3). Such correlations indicate that increasing site Ø stability to physical extremes should increase protective titers elicited upon immunization (Fig. 4A) (*36*). Similarly, correlations between various conformational states or regions of RSV F (Fig. 2) and immunogenicity (Fig. 3) provide design insight into the conformation and regions of RSV F that provide the most protective responses. Specifically, enhancing structural mimicry of antigenic site Ø in its D25-bound conformation appears to be a promising strategy for improving protective antibody responses (Fig. 4B).

We should also be able to estimate the degree to which improvement can be obtained relative to a particular parameter. For example, once a correlation has been established between physical stability or structural mimicry and protective responses, physical stability can be maximized (e.g., to 100% retention of D25 binding) or structural mimicry idealized (e.g., to exact mimicry of the D25-bound conformation) to gain an estimate of the maximal improvement of the elicited protective response relative to that particular parameter. The results (Fig. 4, A and B) suggest that increased structural mimicry would likely not have much effect on immunogenicity but that additional physical stabilization of antigenic site Ø might improve the protective titers by up to fourfold. Independent parameters such as adjuvant, multimerization, delivery vehicle, or immunization regimen offer further avenues for improvement of the elicited response (*37*).

To quantify elicited binding responses, we coupled different variants of RSV F to an Octet biosensor tip and measured their reactivity with elicited sera (Fig. 4C). "Self-reactive" binding responses (with DS-Cav1, DS, or postfusion F on the biosensor tip and sera from animals immunized with DS-Cav1, DS, or postfusion F, respectively) were comparable for DS-Cav1, DS, and postfusion F. To provide insight into the binding responses relative to surfaces that were either shared or unique to DS-Cav1, DS, and postfusion F, we measured "cross-reactive" binding responses, for example, with DS-Cav1 on the biosensor tip and sera from animals immunized with DS or postfusion F, as well as binding responses with "preabsorbed" sera, to which different forms of RSV F had been added (Fig. 4C). We calculated the shared and unique surface areas, computed from crystal structures of DS-Cav1, DS, and postfusion F (fig. S11 and table S3), and analyzed these relative to the 36 measured binding responses in Fig. 4C. Strong correlation was observed between binding responses and calculated surface areas (Fig. 4D). Several outliers involved surfaces unique to DS-Cav1, surfaces that likely comprise antigenic site Ø. Together the results indicate that the quantity of elicited binding antibody was, to a first approximation, proportional to the surface area of the immunogen, independent of whether that immunogen was DS-Cav1, DS, or postfusion F; within this overall similarity, antigenic site Ø elicited ~2 times the titer of binding antibody relative to its surface area. Overall, elicited EC_{50} titers did not correlate with antigenic responses measured against either prefusion or postfusion forms of RSV F but did correlate with the level of prefusion-specific responses, either measured as a difference or as a ratio ($P = 0.005$) between prefusion-specific and postfusion-specific RSV F–directed responses (Fig. 4E) (*38*); the steep slope of this correlation likely reflects the substantially higher neutralization potency observed for prefusion-specific antibodies that target antigenic site Ø (*7*, *39*).

Structural Vaccinology

Structural biology can be used in vaccine development to identify key sites by which to disable a pathogen, to pinpoint residue substitutions that inactivate toxoids, to stabilize select conformations of a subunit antigen, and to determine antibody-antigen complexes, which serve as the basis for epitope-specific strategies of elicitation. Notably, atomic-level control of antigenicity increasingly appears to be within the reach of structure-based design (*16*, *40*, *41*). With complex pathogens like malaria or meningoccocus, antibody-mediated neutralizing activity can be directed against many potential antigens, and vaccine discovery has focused on identifying the best target antigen by methods including genomic analysis or "reverse vaccinology" (*42*–*45*). However, for pathogens such as HIV-1, influenza, or RSV, where neutralizing antibodies act almost exclusively through one or two envelope glycoproteins, a site- or supersite-specific strategy might have advantages. Specifically, a viral site of vulnerability to neutralizing antibody may be more amenable to structure-based design than a viral subunit, while also retaining a higher level of immunogenicity than an epitope-specific scaffold (*46*).

With site-specific vaccine strategies, selection of an appropriate target site is of crucial importance. Elicitation frequency, breadth, and potency are key considerations. Antigenic sites that comprise multiple overlapping epitopes of frequently elicited antibodies may be good targets, because of their expected capacity to elicit high levels of reactive antibodies in the general population. In terms of breadth, site Ø is among the most divergent of the antigenic sites on RSV; however, site Ø–directed antibodies such as D25 are capable of neutralizing most human RSVs, likely because of the relatively low genetic diversity of F among circulating human RSV strains, and both subtype A and B neutralizing activity was potently induced by the stabilized RSV F glycoproteins reported here (table S4). Potency played a key role in our selection of site Ø as a vaccine target, and antigenic analysis of the elicited response (Fig. 4E) indicated potency of elicited antibodies to be crucial to the success of our site Ø–focused approach (*47*). Whether the "neutralization-sensitive site" strategy employed here will have success in other contexts thus depends on virus-specific factors such as circulating viral diversity and required level of neutralizing activity to achieve protection. Nonetheless, many of the lessons learned from our efforts with RSV, such as the importance of examining natural human immune responses and of selecting an appropriate target site, are generally applicable.

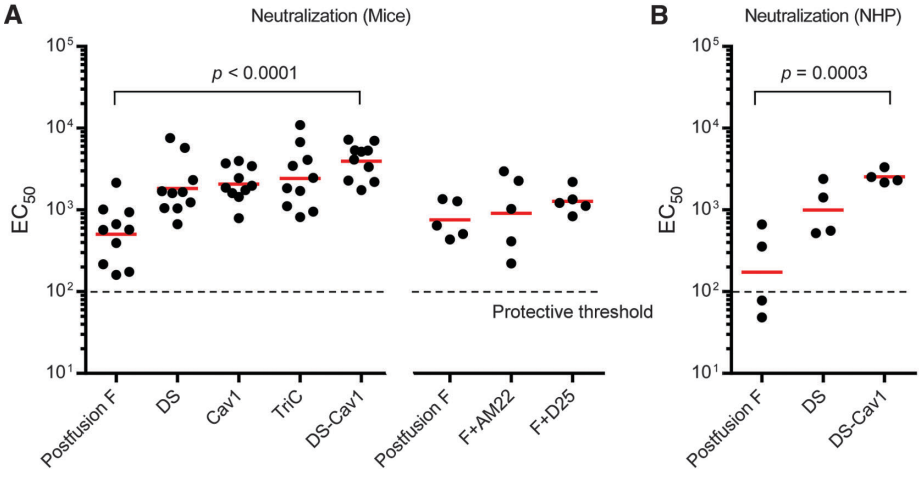

Fig. 3. Immunogenicity of engineered RSV F trimers. RSV F glycoproteins engineered to display antigenic site Ø elicit neutralizing titers significantly higher than those elicited by postfusion F. (**A**) Neutralization titers of sera from mice immunized with 10 μg of RSV F (left). Postfusion F, as well as RSV F bound by antibodies AM22 or D25, were administered at 20 μg of the RSV F–antibody complex per mouse (right). Titers from each mouse are shown as individual black dots, and geometric means are indicated by red horizontal lines. (**B**) Neutralization titers of sera from rhesus macaques (nonhuman primates, NHP) immunized with 50 μg of RSV F glycoprotein variants. Titers from each macaque are shown as individual black dots, and geometric means are indicated by red horizontal lines. Protective threshold (*34*) is indicated by a dotted line, and *P* values are provided for postfusion versus DS-Cav1 as assessed by two-tailed *t* test.

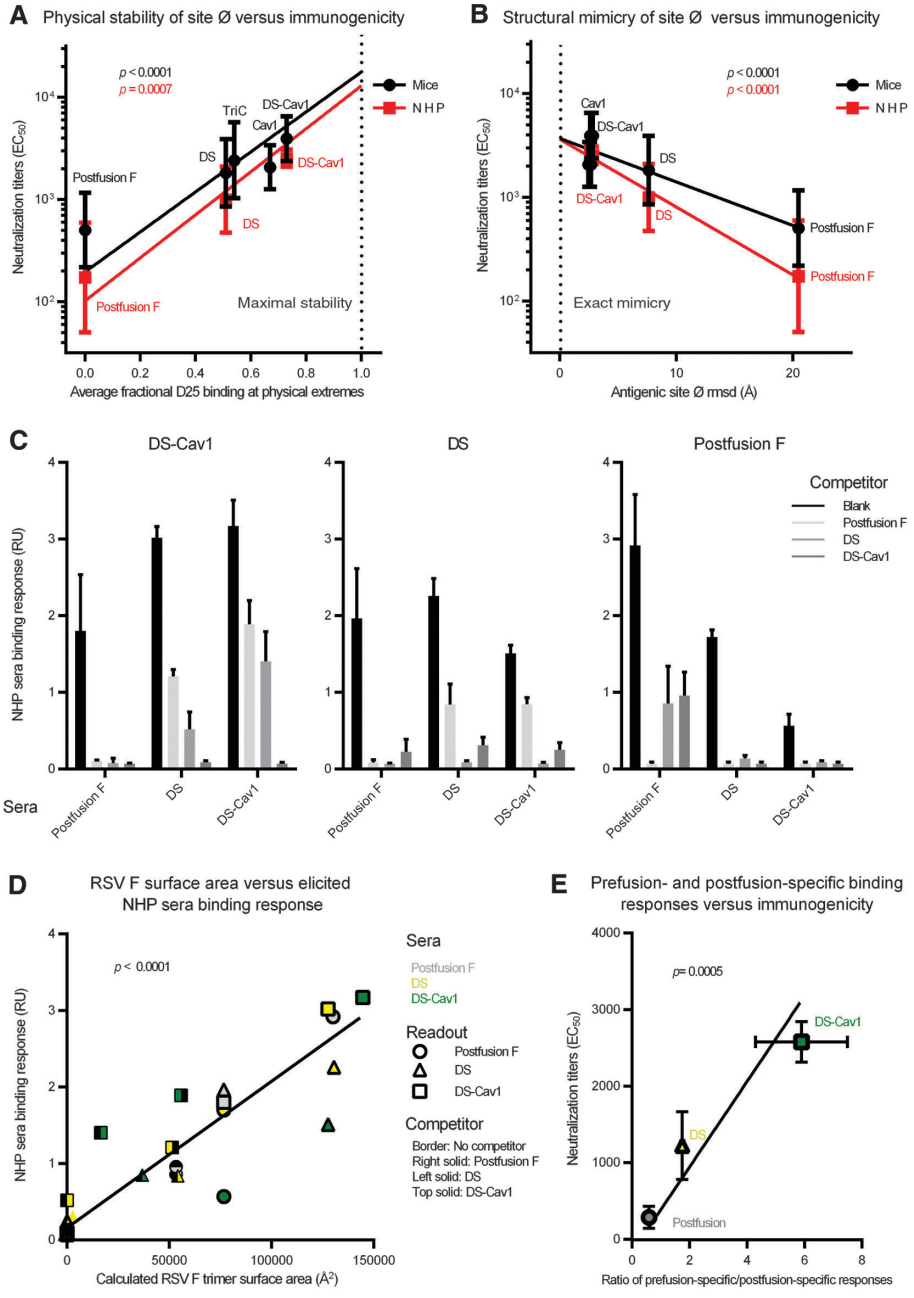

Fig. 4. Informatics of site Ø–stabilized RSV F immunogens. (**A**) Physical stability of site Ø versus immunogenicity. Physical stability (horizontal axis), as determined by the average of seven measurements of D25-retained activity in Table 1, is compared with elicited RSV-protective titers from Fig. 3 (vertical axis). (**B**) Structural mimicry of site Ø versus immunogenicity. Structural mimicry (horizontal axis) is the root-mean-square deviation of atom distances between different unbound RSV F structures (Fig. 2) and the D25-bound RSV F structure for all atoms within 10 Å of D25. This is compared with elicited RSV-neutralizing titers from Fig. 3 (vertical axis). (**C**) Antigenic analysis of sera from immunized macaques. Binding of sera to sensor-tip immobilized DS-Cav1 (left), DS (middle), or postfusion F (right) was measured directly (black bars) or after incubation with excess postfusion F (light gray bars), DS (gray bars), or DS-Cav1 (dark gray bars). The mean responses of four macaque sera are shown, with standard deviations as error bars. Additional analysis of immunized sera is shown in fig. S12. (**D**) Elicited binding responses relative to surface areas for shared or unique portions of immunogens. Surface areas were calculated (fig. S11 and table S3) and compared with binding responses for the 36 response measurements in (C). (**E**) Correlation of immunogenicity and antigenic specificity of immunized macaque sera. The mean EC_{50} neutralization titers (week 6) of the four macaque sera in each group are plotted against the ratio of prefusion-specific/postfusion-specific F binding responses in (C) (*38*).

References and Notes

1. R. Lozano *et al.*, *Lancet* **380**, 2095–2128 (2012).
2. S. Johnson *et al.*, *J. Infect. Dis.* **176**, 1215–1224 (1997).
3. The IMpact-RSV Study Group, *Pediatrics* **102**, 531–537 (1998).
4. L. J. Earp, S. E. Delos, H. E. Park, J. M. White, *Curr. Top. Microbiol. Immunol.* **285**, 25–66 (2005).
5. J. S. McLellan, Y. Yang, B. S. Graham, P. D. Kwong, *J. Virol.* **85**, 7788–7796 (2011).
6. K. A. Swanson *et al.*, *Proc. Natl. Acad. Sci. U.S.A.* **108**, 9619–9624 (2011).
7. J. S. McLellan *et al.*, *Science* **340**, 1113–1117 (2013).
8. L. Liljeroos, M. A. Krzyzaniak, A. Helenius, S. J. Butcher, *Proc. Natl. Acad. Sci. U.S.A.* **110**, 11133–11138 (2013).
9. L. J. Anderson *et al.*, *Vaccine* **31** (suppl. 2), B209–B215 (2013).
10. M. Magro *et al.*, *Proc. Natl. Acad. Sci. U.S.A.* **109**, 3089–3094 (2012).
11. H. Spits, T. Beaumont, RSV-specific binding molecules and means for producing them. Patent Application 12/600,950 (2010).
12. T. Beaumont, A. Q. Bakker, E. Yasuda, RSV specific binding molecule. Patent Application 12/898,325 (2012).
13. D. R. Burton, *Nat. Rev. Immunol.* **2**, 706–713 (2002).
14. T. Zhou *et al.*, *Nature* **445**, 732–737 (2007).
15. G. Ofek *et al.*, *Proc. Natl. Acad. Sci. U.S.A.* **107**, 17880–17887 (2010).
16. J. Jardine *et al.*, *Science* **340**, 711–716 (2013).
17. A. T. McGuire *et al.*, *J. Exp. Med.* **210**, 655–663 (2013).
18. J. S. McLellan *et al.*, *Nat. Struct. Mol. Biol.* **17**, 248–250 (2010).
19. J. S. McLellan *et al.*, *J. Mol. Biol.* **409**, 853–866 (2011).
20. L. Kong *et al.*, *Nat. Struct. Mol. Biol.* **20**, 796–803 (2013).
21. V. P. Efimov *et al.*, *J. Mol. Biol.* **242**, 470–486 (1994).
22. K. A. Miroshnikov *et al.*, *Protein Eng.* **11**, 329–332 (1998).
23. Single-letter abbreviations for the amino acid residues are as follows: A, Ala; C, Cys; D, Asp; E, Glu; F, Phe; G, Gly; H, His; I, Ile; K, Lys; L, Leu; M, Met; N, Asn; P, Pro; Q, Gln; R, Arg; S, Ser; T, Thr; V, Val; W, Trp; and Y, Tyr.
24. Information on materials and methods is available on *Science* Online.
25. RSV F variants were assessed by transient expression in 96-well format (fig. S4). If supernatants retained reactivity with antibodies motavizumab and D25 after 1 week at 4°C, they were expressed by transient transfection of 1 liter of Expi293F cells, purified by use of appended His-tag and StreptagII, and analyzed by size-exclusion chromatography (fig. S7).
26. The inability to express potential interchain double-cysteine substitutions, despite reasonable modeling in the mature prefusion F_1F_2 structure, may indicate that RSV F_0 protomers, before cleavage and removal of peptide 27, adopt substantially different interprotomer conformations.
27. Cavities in the D25-bound RSV F structure were visualized with PyMol using the "Cavities & Pockets Only" option for Surface settings. Amino acid substitutions designed to fill the resulting cavities were identified using the Mutagenesis wizard.
28. M. Pancera *et al.*, *PLOS ONE* **8**, e55701 (2013).
29. The engineered RSV F variants had Cα-root mean square deviations from the D25-bound conformation of 0.7 to 1.5 Å and from the postfusion conformation of approximately 30 Å.
30. Crystallized DS retained ~20% of its D25 recognition relative to crystallized Cav1 (normalized to motavizumab recognition) after 4 months at 20°C, thereby indicating that the crystallized DS was both capable of recognizing D25 as well as converting to a conformation incompatible with D25 binding. By contrast, soluble DS lost all recognition of D25 after 2 months of incubation at 4°C in PBS. We were unable to crystallize DS, which had been heat triggered at 50°C, despite the heat-triggered DS retaining a trimeric state on size exclusion chromatography.

31. Observing Ala107 rather than Arg109 at the C terminus of F_2 is not totally unexpected: Garten and Klenk (*48*) found that an arginine at the cleavage site of influenza hemagglutinin was trimmed by a cellular carboxypeptidase activity.
32. Cα-root mean square deviations of 0.86 Å for 447 residues between Cav1 and DS-Cav1 crystal structures obtained from ammonium sulfate; Cα-root mean square deviations of 0.47 Å for 447 residues of DS-Cav1 in cubic lattices.
33. J. Stetefeld *et al*., *Structure* **11**, 339–346 (2003).
34. When palivizumab (Synagis) is dosed at a concentration of 15 mg/kg, serum levels at trough are ~40 μg/ml, which provides protection in infants from severe disease and protection in cotton rats from RSV infection. In our neutralization assay, ~40 μg/ml of palivizumab yields an EC_{50} of 100.
35. G. J. Nabel, *Science* **326**, 53–54 (2009).
36. By contrast, affinity of RSV F variants for D25 antibody did not show correlation with elicitation of protective titers. Yield of RSV F trimers also did not correlate with protective titers.
37. Flexibility of an antigenic site may increase its immunogenicity by allowing the site to conform to a wider diversity of antibodies. We note in this context that the atomic-mobility factors of antigenic site Ø were among the highest in the RSV F ectodomain.
38. For the "prefusion" form of RSV F, we used the DS-Cav1 stabilized variant of RSV F.
39. It should be possible to deconvolute the elicited response, by using structurally defined probes, as shown with D25 and motavizumab-bound RSV F in fig. S12.
40. P. R. Dormitzer, G. Grandi, R. Rappuoli, *Nat. Rev. Microbiol.* **10**, 807–813 (2012).
41. M. L. Azoitei *et al*., *Science* **334**, 373–376 (2011).
42. I. Delany, R. Rappuoli, K. L. Seib, *Cold Spring Harb. Perspect. Med.* **3**, a012476 (2013).
43. A. Sette, R. Rappuoli, *Immunity* **33**, 530–541 (2010).
44. D. G. Moriel *et al*., *Proc. Natl. Acad. Sci. U.S.A.* **107**, 9072–9077 (2010).
45. M. Mora, C. Donati, D. Medini, A. Covacci, R. Rappuoli, *Curr. Opin. Microbiol.* **9**, 532–536 (2006).
46. Although an epitope-scaffold strategy may not elicit titers as high as a neutralization-sensitive site strategy, for specific antibodies—such as antibody MPE8 (*49*), which is capable of neutralizing not only RSV but other paramyxoviruses including human metapneumovirus—an epitope-specific strategy may suffice.
47. The magnitude of antibody activity is a crucial determinant of how well an individual will be protected following vaccination and how long protective responses will be maintained in infants who have passively acquired antibody from their mothers.
48. W. Garten, H. D. Klenk, *J. Gen. Virol.* **64**, 2127–2137 (1983).
49. D. Corti *et al*., *Nature* **501**, 439–443 (2013).

Acknowledgments: We thank A. M. Salazar for poly-ICLC; J. Stuckey for assistance with figures; I. S. Georgiev and M. Pancera for assistance with immunogen design; G. J. Nabel, R. A. Seder, L. Shapiro, and members of the Structural Biology Section; Structural Bioinformatics Core Section; and Viral Pathogenesis Laboratory at the Vaccine Research Center for helpful comments; and J. Chrzas, J. Gonczy, U. Chinte, and staff at SER-CAT (Southeast Regional Collaborative Access Team) for help with x-ray diffraction data collection. The data presented in this manuscript are tabulated in the main paper and supplementary materials. Atomic coordinates and structure factors of the reported crystal structures have been deposited in the Protein Data Bank under accession codes 4MMQ to 4MMV. Support for this work was provided by the Intramural Research Program (National Institute of Allergy and Infectious Diseases) and the National Natural Science Foundation of China (81161120419 and 812111615). Use of insertion device 22 (SER-CAT) at the Advanced Photon Source was supported by the U.S. Department of Energy, Basic Energy Sciences, Office of Science, under contract W-31-109-Eng-38. H.S. and T.B. are inventors on an international patent application describing the technology used to isolate D25 and AM22 (Means and methods for influencing the stability of antibody producing cells, WO2007067046A1). A.Q.B. and T.B. are inventors on international patent applications for antibody D25 (RSV-specific binding molecules and means for producing them, WO2008147196A2) and antibody AM22 (RSV-specific binding molecule, WO2011043643A1). J.S.M., M.G.J., B.Z., B.S.G., and P.D.K. are inventors on U.S. patent applications describing the use of prefusion-stabilized RSV F glycoproteins as vaccine antigens (Prefusion RSV F proteins and their use, 61/798,389 and 61/863,909). J.S.M., M.C., Z.Z., N.X., and B.S.G. are inventors on a Chinese patent application for antibody 5C4 and its epitope (Anti-RSV high neutralization antibody and the peptide can be used for prevention of RSV infection and related disease, 201310082338.1). Reagents from the NIH are subject to nonrestrictive materials transfer agreements.

Supplementary Materials

www.sciencemag.org/content/342/6158/592/suppl/DC1
Materials and Methods
Figs. S1 to S12
Tables S1 to S4
References (*50*–*61*)

16 July 2013; accepted 25 September 2013
10.1126/science.1243283

REPORTS

Evolution of the Magnetic Field Structure of the Crab Pulsar

Andrew Lyne,[1]* Francis Graham-Smith,[1] Patrick Weltevrede,[1] Christine Jordan,[1] Ben Stappers,[1] Cees Bassa,[1] Michael Kramer[1,2]

Pulsars are highly magnetized rotating neutron stars and are well known for the stability of their signature pulse shapes, allowing high-precision studies of their rotation. However, during the past 22 years, the radio pulse profile of the Crab pulsar has shown a steady increase in the separation of the main pulse and interpulse components at 0.62° ± 0.03° per century. There are also secular changes in the relative strengths of several components of the profile. The changing component separation indicates that the axis of the dipolar magnetic field, embedded in the neutron star, is moving toward the stellar equator. This evolution of the magnetic field could explain why the pulsar does not spin down as expected from simple braking by a rotating dipolar magnetic field.

The Crab pulsar (*1*) originated in the collapse of the core of a massive star in CE 1054, an event that was visible on Earth through the subsequent supernova explosion. Presently rotating at 30 times a second (*2*), intense beams of electromagnetic radiation from the magnetic poles of the neutron star sweep across the Earth (*3*), resulting in a pulsed emission that has been observed since 1969 at radio wavelengths and subsequently at optical, x-ray, and gamma-ray wavelengths. The pulse profile is related to the shape of the beams, which are determined by the magnetic field structure of the underlying star as it rotates (*3*). We have therefore sought changes in the radio pulse profile in order to investigate any evolution in the structure of the stellar magnetic field.

High-quality daily observations of the Crab pulsar (PSR B0531+21, J0534+2200) have been made since 1991 with the 13-m radio telescope at Jodrell Bank Observatory at a frequency of 610 MHz. These measurements are supplemented by less-frequent observations using the 76-m Lovell Telescope at the higher frequency of 1400 MHz, designed to monitor dispersion measure. These data comprise part of a consistent set of pulse timing observations at Jodrell Bank (*4*, *5*) that have provided a complete record of the rotation of the pulsar since 1984 and are available as an ephemeris to other observers (*6*). The radio pulse profile (Fig. 1) consists of a pair of components, the main pulse (MP) at 0° and the interpulse (IP) at 145°, which are closely associated with the components of the profiles observed in the high-energy regimes from optical to TeV gamma rays (*7*). At the comparatively low radio frequency of 610 MHz, there is also a steep-spectrum third component known as the precursor (PC) at −18°. This component is not detectable at 1400 MHz, although another, previously identified component, the low-frequency component (LFC) at −37° (*8*), is seen at both frequencies. The components HFC1 (at 200°) and HFC2 (at 260°) reported before (*8*) also appear in the 1400-MHz profile but are too weak to be addressed in this study.

The temporal evolution of the separation between the MP and other components (*9*) can be seen in Fig. 2 (IP) and Fig. 3 (LFC and PC), and

[1]Jodrell Bank Centre for Astrophysics, School of Physics and Astronomy, University of Manchester, Manchester, M13 9PL, UK. [2]Max Planck Institut für Radioastronomie, Auf dem Hügel 69, 53121 Bonn, Germany.

*Corresponding author. E-mail: andrew.lyne@manchester.ac.uk